Visualizing kinetic pathways of homogeneous nucleation in colloidal crystallization

Peng Tan[1], Ning Xu[2] and Lei Xu[1]★

When a system undergoes a transition from a liquid to a solid phase, it passes through multiple intermediate structures before reaching the final state. However, our knowledge on the exact pathways of this process is limited, mainly owing to the difficulty of realizing direct observations. Here, we experimentally study the evolution of symmetry and density for various colloidal systems during liquid-to-solid phase transitions, and visualize kinetic pathways with single-particle resolution. We observe the formation of relatively ordered precursor structures with different symmetries, which then convert into metastable solids. During this conversion, two major cross-symmetry pathways always occur, regardless of the final state and the interaction potential. In addition, we find a broad decoupling of density variation and symmetry development, and discover that nucleation rarely starts from the densest regions. These findings hold for all of our samples, suggesting the possibility of finding a unified picture for the complex crystallization kinetics in colloidal systems.

Crystallization is an important process in condensed-matter physics and materials science. As liquid changes into solid, evolutions in both symmetry and density take place. However, the exact kinetic pathways across the liquid-to-solid transition remain a focus of debate, with no unified picture so far. Although the classical nucleation theory (CNT) provides a nice framework for understanding crystallization, it has been well recognized that it does not properly describe all aspects of the nucleation process. In the CNT description, the crystallization kinetics proceeds as nucleation and growth of nuclei: small crystals, which have the same symmetry and density as the stable solid, directly emerge from the liquid through spontaneous density fluctuation. In contrast, however, previous studies find rather different results: multiple metastable solids that may differ from the stable solid are observed, with one dominant component prevailing in the nucleation process[1,2]. More specifically, the body-centred cubic (bcc) symmetry dominates the early crystallization in Lennard-Jones and other soft-potential systems[3–8], whereas the random hexagonal close-packed (rhcp) structure is the dominant metastable solid in hard-sphere systems[9–13] (rhcp is a mixture of face-centred cubic (fcc) and hexagonal close-packed (hcp) structures). The kinetic origin of these metastable solids, especially of the dominant component, is an outstanding issue requiring experimental elucidation.

The density variation accompanying such symmetry transformation remains unclear. The traditional view of CNT is that of a simultaneous density and symmetry variation within one step; whereas recent simulations suggest the possibility of either a two-step variation where densification precedes order construction[14], or a gradual transition in both symmetry and density driven by the bond order fluctuation[15,16]. The exact density–symmetry correlation depends on the kinetic transformations among different intermediate structures, which can be best clarified with single-particle-level experiments.

The absence of kinetic information also prevents a clear understanding on the liquid state immediately before crys-tallization. Unlike the conventional picture of a uniformly disordered liquid state, numerical simulations suggest the existence of relatively dense or relatively ordered liquid structures serving as precursors of nuclei[14–20], which may account for an intermediate crystallization step[21–24]. However, the entire picture is far from clear. How the liquid passes through the precursor state to evolve into metastable solids remains a big mystery—even the direct observation of precursors in three-dimensional real space is still missing. To tackle this mystery, visualizing the crystallization kinetics again plays an essential role.

In this study, we report single-particle level measurements on the kinetics of three-dimensional colloidal crystallization, for both symmetry and density transformations. To find the universal kinetics, extensive studies across different final states and interaction potentials are performed. Colloidal systems are used owing to their similar phase-transition behaviours as atomic and molecular systems, and their large particle sizes enabling single-particle level visualization[12,25–32]. We directly observe relatively ordered liquid structures behaving as precursors, out of which small nuclei emerge. These precursors exhibit local orders close to hcp, bcc and fcc symmetries, and subsequently convert into these metastable solids. During this precursor-to-solid conversion, interestingly, two major cross-symmetry pathways are universally observed: hcp-like precursors to bcc metastable solid and hcp-like precursors to fcc metastable solid. These major pathways could explain the kinetic origin of the dominant metastable solid. In the density evolution, we discover a strong decoupling between density variation and symmetry development, and demonstrate that initial nucleation rarely starts from the densest regions of our samples.

Our system is made up of poly(methyl methacrylate) colloids with diameter $\sigma = 2.2\,\mu\text{m}$ and a polydispersity of less than 2.5%, suspended in a density- and refractive-index-matched solvent. The particles carry charges and form Wigner crystals at low concentrations[33,34]. We fix the sample concentration at 17%, which avoids particle–particle contact and ensures soft-

[1]Department of Physics, The Chinese University of Hong Kong, Hong Kong, China, [2]CAS Laboratory of Soft Matter Chemistry, Hefei National Laboratory for Physical Sciences at Microscale and Department of Physics, University of Science and Technology of China, Hefei 230026, China.
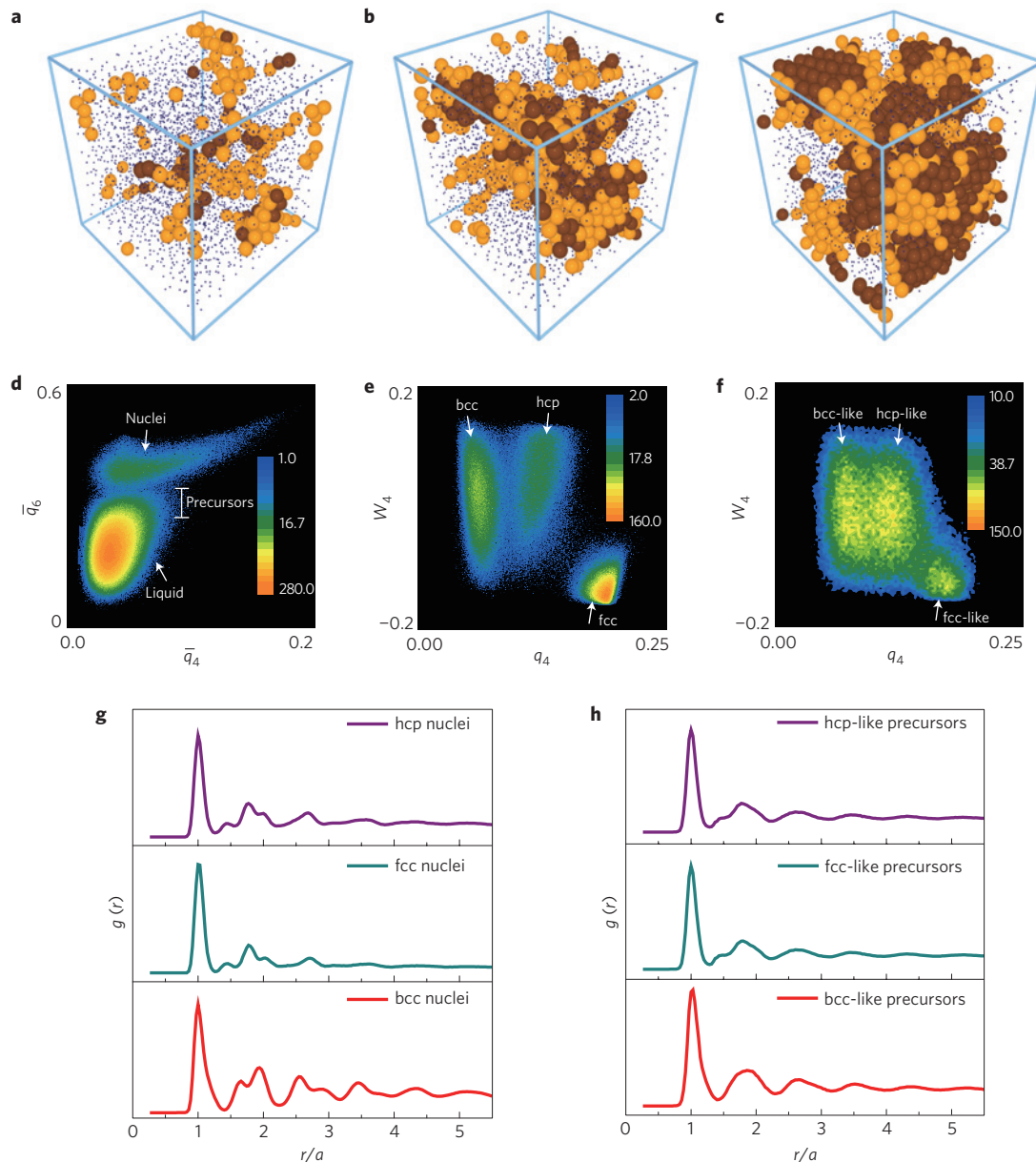*e-mail: xulei@phy.cuhk.edu.hk

Figure 1 | Structures of nuclei and precursors in early crystallization. a–c, Precursor-mediated crystallization in a bcc-stable ($\kappa^{-1} = 960$ nm) system. The brown spheres represent nucleus particles, and the orange spheres indicate relatively ordered liquid particles that we define as precursors. The blue dots are normal liquid particles. At the beginning of nucleation (**a,** $\phi_{nuclei} = 1.9\%$, $\phi_{precursor} = 5.6\%$, $t = 240$ s), nucleated embryos emerge from clusters of precursors. During the subsequent development around critical (**b,** $\phi_{nuclei} = 7.1\%$, $\phi_{precursor} = 11.6\%$, $t = 2,640$ s) and post-critical (**c,** $\phi_{nuclei} = 21.4\%$, $\phi_{precursor} = 20.4\%$, $t = 6,480$ s) nucleus sizes, precursors are continuously created around nuclei. **d,** Particle count (logarithmic scale) in the $\bar{q}_6$–$\bar{q}_4$ plane in the early crystallization (solid fraction ∼ 5%). The upper group with higher $\bar{q}_6$ is composed of nucleus particles, and the lower group is composed of liquid particles. Within the liquid group, relatively ordered particles with $\bar{q}_6 > 0.27$ are defined as precursors. **e,** Nucleus count (logarithmic scale) in the W_4–q_4 plane reveals three metastable crystalline symmetries: bcc, hcp and fcc. **f,** W_4–q_4 plot of precursors (logarithmic scale) reveals bcc-like, hcp-like and fcc-like precursors in the liquid stage. **g,h,** Radial distribution function for the three types of nucleus and precursor symmetry. r is renormalized by the average particle distance, a. A good match in the main peaks between **g** and **h** suggests a structural similarity between precursors and nuclei.

repulsive potential (Methods). By tuning the Debye screening length, κ^{-1}, and the surface charge, Z, we can obtain bcc-stable and fcc-stable crystals[33,35]. The phase diagram is shown in Supplementary Fig. 1A. The adjustable stable states offer the opportunity to study kinetic pathways for various transition situations. We shear-melt colloidal crystals and record the recrystallization process immediately after agitation, at a supercooling of $\Delta T = T_m - T = 0.2T_m$ to $0.4T_m$, with T_m being the melting temperature (Methods).

Three symmetries in precursors and nuclei

By inspecting the local bond order parameters (shown later), we can specify highly ordered nucleus particles and relatively ordered liquid particles (in comparison with normal liquid particles), as shown respectively by the dark-brown and light-brown spheres in Fig. 1a–c (Supplementary Movie 1): at the beginning of nucleation in Fig. 1a, small nuclei (dark brown) emerge from relatively ordered liquid structures (light brown) that serve as precursors of solid. Moreover, such precursors are continuously created in the

subsequent development, as demonstrated by Fig. 1b around the stage of critical nucleus size and Fig. 1c for the post-critical stage. Precursors wrap the nuclei like a layer of coating and account for an intermediate step in the liquid–solid transition[14–17,19,20].

To characterize the local order of any particle i, we measure its local bond order parameters,

$$q_l(i) = \left(\frac{4\pi}{2l+1} \Sigma_{m=-l}^{m=l} |q_{l,m}(i)|^2 \right)^{1/2}$$

$$W_l(i) = \Sigma_{m_1,m_2,m_3=0}^{l} \begin{pmatrix} l & l & l \\ m_1 & m_2 & m_3 \end{pmatrix} \frac{q_{l,m_1}(i)q_{l,m_2}(i)q_{l,m_3}(i)}{|q_l(i)|^3}$$

and the coarse-grained bond order parameters, $\bar{q}_l(i) = ((4\pi/(2l+1))\Sigma_{m=-l}^{m=l}|\bar{q}_{l,m}(i)|^2)^{1/2}$. Here $q_{l,m}(i) = (1/Nb(i))\Sigma_{j=1}^{Nb(i)} Y_{l,m}(\theta_{i,j}, \phi_{i,j})$, with $Nb(i)$ the number of neighbours of particle i and $Y_{l,m}(\theta_{i,j}, \phi_{i,j})$ spherical harmonics with $m \in [-l,l]$; $\theta_{i,j}$ and $\phi_{i,j}$ are the polar and azimuthal angles of the vector $\mathbf{r}_{ij} = \mathbf{r}_i - \mathbf{r}_j$ with $\mathbf{r}_i$ the position vector of particle i and $\mathbf{r}_j$ the position vector of any neighboring particle j. $\bar{q}_{l,m}(i) = (1/(Nc(i)+1))\Sigma_{j=0}^{Nc(i)} q_{l,m}(j)$, with $Nc(i) \leq Nb(i)$ the number of neighbours that are in the same phase (liquid or solid) as particle i. The sum over j runs from 0 to $Nc(i)$ to include the particle i itself ($j = 0$) and the $Nc(i)$ neighbours in the same phase (see Supplementary Information for more information[15,36–38]). Good statistics is obtained by locating more than 2×10^6 particles at 50 different regions within the same sample, in the early crystallization stage (solid fraction $\sim 5\%$). A clear distinction between nuclei and liquid is demonstrated by the number distribution of all particles in the $\bar{q}_6$–$\bar{q}_4$ plane in Fig. 1d: the upper group with larger $\bar{q}_6$ is composed of nucleus particles; the lower group with smaller $\bar{q}_6$ is composed of liquid particles. Within the liquid group, we further pick out the particles with relatively high bond order, $\bar{q}_6 > 0.27$, as the light-brown precursors shown in Fig. 1a–c. According to the two-step nucleation theory, precursors are dense structures with a symmetry lower than solid structures[17,18,20,22]. Our precursors are therefore defined as the particles with relatively high local order ($\bar{q}_6 > 0.27$) but below the level of solid structures (solid bond number $\xi < 7$; ref. 37), agreeing with ref. 15. With this definition ($\bar{q}_6 > 0.27$ and $\xi < 7$), the precursors also have densities higher than normal liquid (see Supplementary Fig. 4D), which is consistent with previous simulations[17,18,20,22]. Note that we can further vary the threshold value of 0.27 to numbers between 0.27 and 0.30, and obtain qualitatively similar results, confirming that the precursor properties do not depend on the choice of exact threshold values.

Several crystalline symmetries appear as we further analyse the local order of nuclei and precursors. For nuclei, three distinct symmetries—bcc, hcp and fcc—are illustrated by the W_4–q_4 plot in Fig. 1e. Clearly, nuclei at the early stage are composed of various components[12], which evolve into one stable solid during much later development. Moreover, the same analysis on precursors reveals this symmetry differentiation even before the solid formation: there exist bcc-like, hcp-like and fcc-like precursors whose local structures are similar to the corresponding nuclei, as shown in Fig. 1f and Supplementary Fig. 4C. For the first time, the experiment reveals multiple symmetries emerging in precursors within the liquid stage, which behave as the 'seeds' of the multiple metastable solids and thus account for their kinetic origins.

To verify our symmetry analysis, we plot the radial distribution function, $g(r)$, for the three types of nucleus symmetry in Fig. 1g: all peaks match precisely with the ideal crystals, confirming the validity of our bond order analysis (note that hcp and fcc have similar $g(r)$ as expected). Moreover, we find a good match in the main peaks between the precursors (Fig. 1h) and the corresponding nuclei (Fig. 1g), confirming their underlying structural connection. Owing to this structural similarity, the existence of precursors at the

liquid/solid interface may markedly reduce the interfacial tension and promote the rate of nucleation[12,15]. A small surface tension is also consistent with the ramified nucleus profile observed in the early crystallization stage both in this experiment (Fig. 1a,b as an example) and in a previous study[12].

In addition, we clarify one important point: the local order in precursors revealed by us is quite short-ranged, typically extending only to the first shell (the central particle plus its neighbours). When longer ranges are involved, however, the bulk phase of precursor clusters is quite amorphous, owing to the mixing and interfering of multiple components (Fig. 2a). In comparison to previous studies, our precursor definition is similar to the one in ref. 15, but is probably only part of the precursors defined in some other studies[17,18,20,22], which may also contain a truly amorphous fraction. To study this truly amorphous fraction, dynamic investigations regarding the lifetime of dense amorphous clusters would be needed. In conclusion, the precursors in our study exhibit multiple local orders at short range, but are amorphous at intermediate and long ranges (see more details in Supplementary Section IIC, page 10–15).

Kinetic pathways during precursor-to-solid conversion

Our experiment confirms the existence of precursors, which exhibit various symmetries and convert into different metastable solids. However, the symmetry transformation during the precursor-to-solid conversion requires further illumination. To visualize the process, we colour the three symmetries differently and demonstrate their evolutions in Fig. 2a–c (Supplementary Movie 2): at the very beginning in Fig. 2a, the hcp symmetry (nuclei + precursors, purple spheres) dominates the other two, but the bcc symmetry (red spheres) catches up around the critical nucleus size in Fig. 2b, and later dominates the system (Fig. 2c). This particular sample eventually develops into a bcc crystal.

The system evolves from hcp-dominant to bcc-dominant, indicating transformations across different symmetries. To figure out the transformation pathways, we track the relative fractions of different symmetries with respect to time, for both precursors and nuclei. The typical result for a bcc-stable system is demonstrated in Fig. 2d: for all three symmetries, the precursor (open symbols) and nucleus (close symbols) curves are roughly parallel, demonstrating their close correlation. However, a gap also exists between the two, revealing cross-symmetry transformations during the precursor-to-solid conversion. More specifically, in the hcp panel the precursor curve is higher than the nucleus one, indicating an extra fraction of hcp-like precursors that must convert into other types of nucleus. Correspondingly, in the bcc and fcc panels excess fractions of nuclei (instead of precursors) are found, reconfirming the conversion from hcp-like precursors. Therefore, our data indicate two cross-symmetry pathways during the precursor-to-solid conversion: hcp-like precursors to bcc nuclei and hcp-like precursors to fcc nuclei. The same kinetic pathways are also observed in a typical fcc-stable system, as shown in Fig. 2e. In addition, hard-sphere systems exhibit the same behaviour (see Supplementary Fig. 12) as well, demonstrating the general validity of the two cross-symmetry pathways.

To visualize the pathways directly, we illustrate all possible conversions between different types of precursor and nucleus in the $\bar{q}_6$–q_4 plane in Fig. 2f: the $\bar{q}_6$ values are used to distinguish nuclei from precursors, and the q_4 values are used to distinguish different symmetries. The lower cluster indicates precursors, the upper cluster represents nuclei, and the connection in between is from the particles caught during the precursor-to-nucleus conversion that directly visualizes the kinetic pathway. Clearly, a pathway always exists for a conversion within the same symmetry as demonstrated by the three corresponding images in Fig. 2f (upper-left to lower-right diagonal), which corroborates a previous simulation[16].
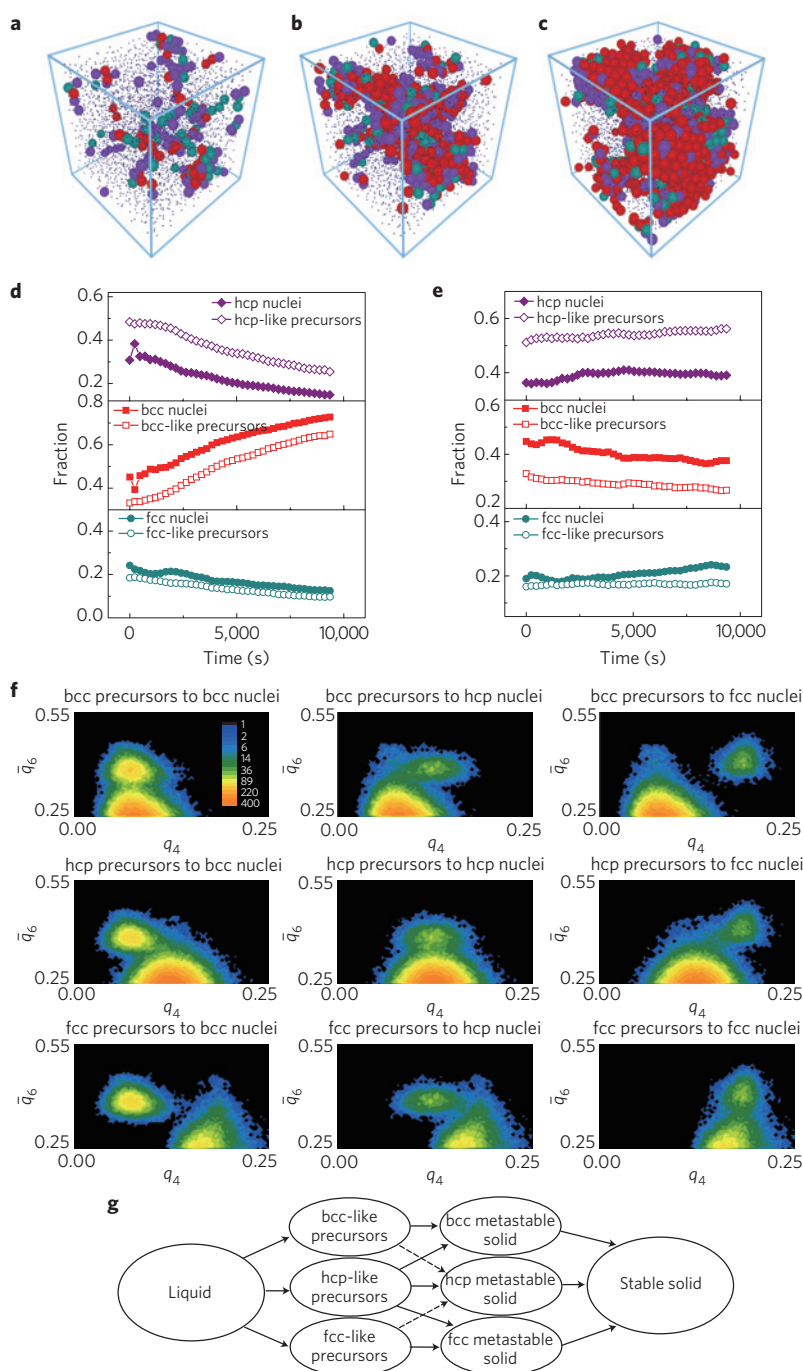
Figure 2 | Kinetic pathways during crystallization. a–c, Time evolution of different symmetries. The purple spheres indicate hcp nuclei and hcp-like precursors, the red spheres represent bcc nuclei and bcc-like precursors, and the green spheres fcc nuclei and fcc-like precursors. The three configurations are identical to the ones in Fig. 1a–c. The hcp symmetry (purple) initially dominates (**a**, $\phi_{nuclei} = 1.9\%$, $\phi_{precursor} = 5.6\%$, $t = 240$ s), but the bcc symmetry (red) then catches up (**b**, $\phi_{nuclei} = 7.1\%$, $\phi_{precursor} = 11.6\%$, $t = 2,640$ s) and eventually takes over (**c**, $\phi_{nuclei} = 21.4\%$, $\phi_{precursor} = 20.4\%$, $t = 6,480$ s). **d**, Relative fractions of precursors (open symbols) and nuclei (filled symbols) for every symmetry in a bcc-stable ($\kappa^{-1} = 960$ nm) system. The precursor and nucleus curves are mostly parallel, indicating their strong correlation. In the hcp panel, the precursor curve is above the nucleus one, whereas in bcc and fcc panels, the precursor curve is below the nucleus one. This indicates two kinetic pathways from the hcp-like precursors to bcc and fcc nuclei. The critical nucleus size is reached around $t = 2,640$ s. **e**, The same pathways are also observed in an fcc-stable ($\kappa^{-1} = 520$ nm) system. The critical nucleus size is reached around $t = 2,400$ s. **f**, Direct visualization of kinetic pathways in the $\bar{q}_6$–q_4 plane (logarithmic scale). Each image illustrates the conversion from one type of precursor to one type of nucleus. The lower cluster indicates precursors, the upper cluster represents nuclei, and the connection in between visualizes the pathway. For conversions within the same symmetry, a pathway always exists. For cross-symmetry conversions, there are two major pathways from hcp precursors to bcc and fcc nuclei and two weak pathways from bcc and fcc precursors to hcp nuclei. There is essentially no pathway between the fcc and bcc symmetries. **g**, Summary of kinetics during the precursor-mediated crystallization. Solid lines indicate the major pathways, and dashed lines represent the minor pathways.
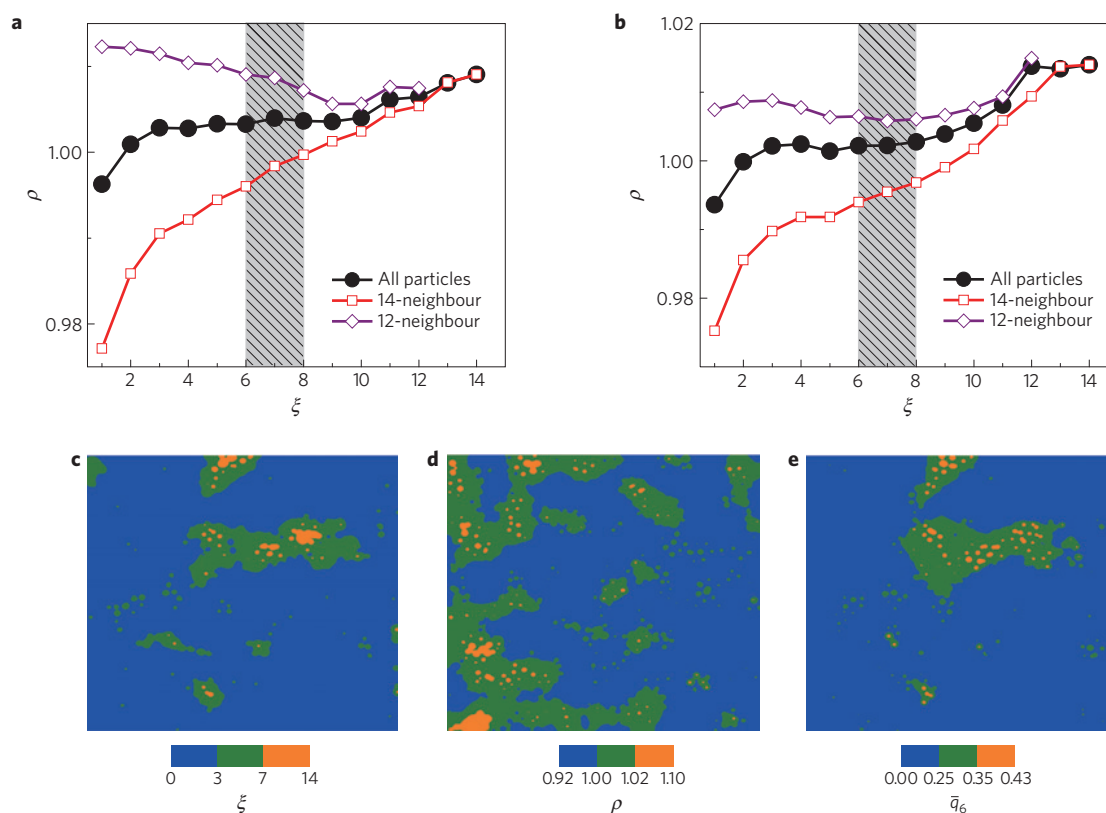
Figure 3 | Local density evolution throughout crystallization. a, ρ, versus ξ, in a bcc-stable ($\kappa^{-1} = 960$ nm) system. The solid symbols represent the average local density as a function of the local order development, and the hatched grey region indicates the liquid-to-solid transition boundary. As ξ increases, ρ first experiences a rapid increase that corresponds to the precursor formation, followed by a broad plateau ($3 < \xi < 10$) that corresponds to the precursor-to-solid conversion. In particular, no density jump is observed at the hatched area of the liquid/solid transition boundary, in sharp contrast to the CNT description. The second increase occurs at $\xi > 10$ as the local order undergoes the final perfection in nuclei. The open symbols demonstrate the 14-neighbour branch (bcc) and the 12-neighbour branch (hcp and fcc). At low ξ there exists a large gap between the two branches, which diminishes with the increase of order. Before the order is fully constructed, the 14-neighbour branch is always below the 12-neighbour one, indicating the lower density of the bcc structure. However, eventually the 14-bond (bcc) crystal becomes denser than the 12-bond (fcc and hcp) crystal. **b**, The same measurements in an fcc-stable ($\kappa^{-1} = 520$ nm) system. A similar three-stage correlation is observed, but the end point of the 12-neighbour branch is now higher than the end point of the 14-neighbour branch. **c–e**, Snapshots of the spatial distributions for the ξ (**c**), ρ (**d**), $\bar{q}_6$ (**e**). The data are taken in a 5-μm-thick slice at the early crystallization stage. Clearly the density plot has a poor correlation with the other two, indicating that the nucleation events (regions with high ξ and $\bar{q}_6$ values) rarely start from the densest regions.

More interesting, cross-symmetry pathways previously never reported also appear. Two strong pathways from hcp precursors to bcc nuclei and fcc nuclei are revealed in the second row, consistent with Fig. 2d,e. At the same time, two weak pathways from bcc precursors and fcc precursors to hcp nuclei are also found, although overwhelmed by the effect from the two strong ones just mentioned. For the interaction between bcc and fcc symmetries, there is essentially no pathway during the conversion. These kinetic pathways are universally observed in all of our soft-repulsive systems.

In soft-repulsive systems, we observe dominant hcp-like precursors initially[15,16], which can subsequently convert into bcc and fcc nuclei through two cross-symmetry pathways. However, the pathway to bcc nuclei is much more significant, as demonstrated by its much stronger magnitude (Fig. 2f, second row, the leftmost image compared with the rightmost image). Correspondingly, bcc symmetry dominates the early metastable solid phase in both our soft-repulsive samples and the systems previously studied[2–7]. Therefore, we propose that the dominant cross-symmetry pathway probably leads to the dominant metastable solid in early crystallization. To further test this scenario, we perform the same measurements in hard-sphere systems, whose dominant metastable solid is rhcp (mixture of fcc and hcp) instead of bcc (refs 12,13). As expected, the dominant pathway changes accordingly: the hcp-like precursors now mainly transfer into fcc nuclei instead of bcc, as fcc is one important component of the rhcp structure (see Supplementary Fig. 12). Both the soft-repulsive and hard-sphere experiments are consistent with our newly proposed scenario, which explains the kinetic origin of the dominant metastable solid in early crystallization.

We summarize our crystallization kinetics in Fig. 2g. As the temperature drops below the melting point, precursors emerge out of the liquid, with the hcp-like component dominating the bcc-like and the fcc-like ones. These precursors then convert into metastable solids. Besides the conversion within the same symmetry, interestingly, cross-symmetry pathways also exist: there are two major ones from hcp-like precursors to bcc and fcc nuclei, and two minor ones from bcc-like and fcc-like precursors to hcp nuclei, as represented by the solid and dashed lines respectively. The effect of major pathways overwhelms the effect of minor ones. Eventually all metastable solids evolve into the stable solid (We find that the dominant solid phase in our experiments is bcc ($\lambda \sim 960$ nm) or rhcp ($\lambda \sim 520$ nm) after several days).

Density–symmetry correlation

In the process of crystallization, the establishment of crystalline order is naturally accompanied by density change. We illustrate their correlation by directly measuring the variation of local density with respect to the development of local order. The local density, ρ, is determined by the Voronoi diagram ($\rho = 1$ corresponds to the system average); and the local order is quantified by the solid bond number, ξ (see Supplementary Information for the exact definition). Typically, a larger ξ indicates a better crystalline order. Good statistics is obtained from measurements of more than 10^6 particles in the early crystallization stage (solid fraction $\sim 5\%$). At each solid bond number, we obtain the average local density and illustrate their correlation in the ρ–ξ plot.

A typical ρ–ξ dependence is shown by the solid symbols in Fig. 3a for a bcc-stable system. Clearly there exists a density plateau over a broad range of local order, $3 \leq \xi \leq 10$, indicating very little density change against a significant development of order. In particular, across the hatched area of the liquid/solid boundary ($6 \leq \xi \leq 8$), ρ does not experience any abrupt increase, in sharp contrast to the density jump described in the classical nucleation theory. Significant densification occurs only at either quite early ($\xi < 3$) or rather late ($\xi > 10$) stages of local order construction, and corresponds respectively to the initial formation of precursors and the final perfection of local order. We note that particles with $3 \leq \xi \leq 6$ largely overlap with the precursor particles defined previously (see their similar $g(r)$ in Supplementary Fig. 6). Consequently, our experiment reveals a rather complex three-stage correlation for density and symmetry development: initially they grow simultaneously during the formation of precursors ($\xi < 3$), followed by a decoupling plateau throughout precursor-to-solid conversion ($3 \leq \xi \leq 10$), and then the simultaneous growth reappears for the final perfection of local order ($\xi > 10$). This three-stage trend has never been reported previously and requires further theoretical explanation.

Different symmetries and structures emerge as early as in the liquid stage, and therefore we illustrate their density variations separately as well. We can divide the densities of most particles ($>98\%$) into two branches: the 14-neighbour branch (bcc-like) and the 12-neighbour branch (fcc-like and hcp-like), as shown by the open symbols in Fig. 3a. The two branches exhibit a large difference at low ξ, which diminishes as crystalline order increases. Moreover, before the order is fully constructed, the 14-neighbour branch is always below the 12-neighbour one, indicating a lower density for the bcc-like structure. As we observe a major pathway from hcp-like precursors to bcc nuclei in the soft-repulsive systems, it indicates a conversion from the high-density branch to the low-density one. This conversion apparently lowers the high-density branch, and raises the low-density one, but keeps the average density largely unchanged, as revealed by the plateau of solid symbols. Similar results are also observed in the fcc-stable systems shown in Fig. 3b, except with two minor differences: there is a sharper density increase after the plateau; and the fully developed fcc crystal (that is, the end point of the upper branch) is denser than the bcc counterpart (that is, the end point of the lower branch) whereas the opposite is true in Fig. 3a.

Over a broad range of order construction, a decoupling plateau between density variation and symmetry development is observed, especially at the liquid-to-solid transition boundary ($6 \leq \xi \leq 8$). This discrepancy with the classical picture is even more apparent when we compare the spatial distributions of ξ and ρ in the early crystallization stage: very little correlation is found between the nucleation events indicated by ξ in Fig. 3c and the dense regions specified by ρ in Fig. 3d. The densest regions ($\rho > 1.02$, orange areas) are significantly denser than the nuclei ($\rho \sim 1.01$), and appear mostly at disordered locations. At the same time, the local density fluctuations in both space and time are more than 5%, much larger than the density mismatch between liquid and nuclei (1%–2%). To further test this result, we plot the spatial distribution of local bond order, $\bar{q}_6$, in Fig. 3d, and again find very little correlation with the density plot in Fig. 3d. These results unambiguously demonstrate that nucleation events do not start from the densest regions, in sharp contrast to the conventional picture of nucleation. However, the similarity between Fig. 3c and Fig. 3e indicates a strong correlation between the nucleation events and the local bond order[15,16].

Discussion

One important question remains unclear: why do the hcp-like precursors dominate initially? We believe this is due to the common feature of clusters of tetrahedra adjacent by faces, which widely appear in both the disordered liquid[39] and the hcp-like precursors. This structural similarity makes the transformation to hcp-like precursors a major first step. Subsequently, the local hcp-like symmetry converts into other symmetries through slight deformations: a shear parallel to the hexagonal plane can result in fcc symmetry whereas an in-plane compression (or stretch) may lead to bcc structure. Both approaches involve only locally small movements with little energy cost, but they produce significant changes in symmetry. The underlying inhomogeneous stresses may come from the surface tension of ramified liquid/solid interfaces, as supported by the observation that symmetry conversion mainly occurs at this interface. However, this picture is largely qualitative and calls for further study.

Moreover, the density fluctuations at the single-particle level exceed the liquid–solid density mismatch substantially, implying that local structures can easily fluctuate in and out of the solid density. Combining this with the observation that nucleation rarely starts from the densest regions, we suspect that density fluctuation may not be the main driving factor for our crystallization process; instead the local bond order fluctuation could be a reasonable candidate[16]. Illustrating these emerging questions should shed new light on the conventional picture of crystallization.

Methods

References

1. Ostwald, W. Studien über die Bildung und Umwandlung fester Körper. 1. Abhandlung: Übersättigung und Überkaltung. *Z. Phys. Chem.* **22,** 289–330 (1897).
2. Alexander, S. & McTague, J. Should all crystals be bcc? Landau theory of solidification and crystal nucleation. *Phys. Rev. Lett.* **41,** 702–705 (1978).

3. Ten Wolde, P. R., Ruiz-Montero, M. J. & Frenkel, D. Numerical evidence for bcc ordering at the surface of a critical fcc nucleus. *Phys. Rev. Lett.* **75,** 2714–2717 (1995).
4. Ten Wolde, P. R., Ruiz-Montero, M. J. & Frenkel, D. Numerical calculation of the rate of crystal nucleation in a Lennard-Jones system at moderate undercooling. *J. Chem. Phys.* **104,** 9932–9947 (1996).
5. Shen, Y. C. & Oxtoby, D. W. bcc symmetry in the crystal-melt interface of Lennard-Jones fluids examined through density functional theory. *Phys. Rev. Lett.* **77,** 3585–3588 (1996).
6. Auer, S. & Frenkel, D. Crystallization of weakly charged colloidal spheres: A numerical study. *J. Phys. Condens. Matter* **14,** 7667–7680 (2002).
7. Moroni, D., ten Wolde, P. R. & Bolhuis, P. G. Interplay between structure and size in a critical crystal nucleus. *Phys. Rev. Lett.* **94,** 235703 (2005).
8. Russo, J. & Tanaka, H. Selection mechanism of polymorphs in the crystal nucleation of the Gaussian core model. *Soft Matter* **8,** 4206–4215 (2012).
9. Pusey, P. N. & van Megen, W. Phase behaviour of concentrated suspensions of nearly hard colloidal spheres. *Nature* **320,** 340–342 (1986).
10. Pusey, P. N. *et al.* Structure of crystals of hard colloidal spheres. *Phys. Rev. Lett.* **63,** 2753–2756 (1989).
11. Zhu, J. *et al.* Crystallization of hard-sphere colloids in microgravity. *Nature* **387,** 883–885 (1997).
12. Gasser, U., Weeks, E. R., Schofield, A., Pusey, P. N. & Weitz, D. A. Real-space imaging of nucleation and growth in colloidal crystallization. *Science* **292,** 258–262 (2001).
13. Auer, S. & Frenkel, D. Prediction of absolute crystal-nucleation rate in hard-sphere colloids. *Nature* **409,** 1020–1023 (2001).
14. TenWolde, P. R. & Frenkel, D. Enhancement of protein crystal nucleation by critical density fluctuations. *Science* **277,** 1975–1978 (1997).
15. Kawasaki, T. & Tanaka, H. Formation of a crystal nucleus from liquid. *Proc. Natl Acad. Sci. USA* **107,** 14036–14041 (2010).
16. Russo, J. & Tanaka, H. The microscopic pathway to crystallization in supercooled liquids. *Sci. Rep.* **2,** 505 (2012).
17. Schilling, T., Schöpe, H. J., Oettel, M., Opletal, G. & Snook, I. Precursor-mediated crystallization process in suspensions of hard spheres. *Phys. Rev. Lett.* **105,** 025701 (2010).
18. Tóth, G. I., Pusztai, T., Tegze, G., Tóth, G. & Gránásy, L. Amorphous nucleation precursor in highly nonequilibrium fluids. *Phys. Rev. Lett.* **107,** 175702 (2011).
19. Lechner, W., Dellago, C. & Bolhuis, P. G. Role of the prestructured surface cloud in crystal nucleation. *Phys. Rev. Lett.* **106,** 085701 (2011).
20. Lutsko, J. F. & Nicolis, G. Theoretical evidence for a dense fluid precursor to crystallization. *Phys. Rev. Lett.* **96,** 046102 (2006).
21. Martin, S., Bryant, G. & van Megen, W. Crystallization kinetics of polydisperse colloidal hard spheres: Experimental evidence for local fractionation. *Phys. Rev. E* **67,** 061405 (2003).
22. Schöpe, H. J., Bryant, G. & van Megen, W. Two-step crystallization kinetics in colloidal hard-sphere systems. *Phys. Rev. Lett.* **96,** 175701 (2006).
23. Iacopini, S., Palberg, T. & Schöpe, H. J. Crystallization kinetics of polydisperse hard-sphere-like microgel colloids: Ripening dominated crystal growth above melting. *J. Chem. Phys.* **130,** 084502 (2009).
24. Savage, J. R. & Dinsmore, A. D. Experimental evidence for two-step nucleation in colloidal crystallization. *Phys. Rev. Lett.* **102,** 198302 (2009).
25. Larsen, A. E. & Grier, D. G. Like-charge attractions in metastable colloidal crystallites. *Nature* **385,** 230–233 (1997).
26. Weeks, E. R., Crocker, J. C., Levitt, A. C., Schofield, A. & Weitz, D. A. Three-dimensional direct imaging of structural relaxation near the colloidal glass transition. *Science* **287,** 627–631 (2000).
27. Anderson, V. J. & Lekkerkerker, H. N. Insights into phase transition kinetics from colloid science. *Nature* **416,** 811–815 (2002).
28. Schall, P., Cohen, I., Weitz, D. A. & Spaepen, F. Visualization of dislocation dynamics in colloidal crystals. *Science* **305,** 1944–1948 (2004).
29. Alsayed, A. M., Islam, M. F., Zhang, J., Collings, P. J. & Yodh, A. G. Premelting at defects within bulk colloidal crystals. *Science* **309,** 1207–1210 (2005).
30. Savage, J. R., Blair, D. W., Levine, A. J., Guyer, R. A. & Dinsmore, A. D. Imaging the sublimation dynamics of colloidal crystallites. *Science* **314,** 795–798 (2006).
31. Lu, P. J., Zaccarelli, E., Ciulla, F., Schofield, A. B., Sciortino, F. & Weitz, D. A. Gelation of particles with short-range attraction. *Nature* **453,** 499–503 (2008).
32. Wang, Z. R., Wang, F., Peng, Y., Zheng, Z. Y. & Han, Y. L. Imaging the homogeneous nucleation during the melting of superheated colloidal crystals. *Science* **338,** 87–90 (2012).
33. Leunissen, M. E. *et al.* Ionic colloidal crystals of oppositely charged particles. *Nature* **437,** 235–240 (2005).
34. Tan, P., Xu, N., Schofield, A. & Xu, L. Understanding the low-frequency quasilocalized modes in disordered colloidal systems. *Phys. Rev. Lett.* **108,** 095501 (2012).
35. Hynninen, A. & Dijkstra, M. Phase diagrams of hard-core repulsive Yukawa particles. *Phys. Rev. E* **68,** 021407 (2003).
36. Steinhardt, P. J., Nelson, D. R. & Ronchetti, M. Bond-orientational order in liquids and glasses. *Phys. Rev. B* **28,** 784–805 (1983).
37. Ten Wolde, P., Ruiz-Montero, M. J. & Frenkel, D. Simulation of homogeneous crystal nucleation close to coexistence. *Faraday Discuss.* **104,** 93–110 (1996).
38. Lechner, W. & Dellago, C. Crystal structures based on averaged local bond order parameters. *J. Chem. Phys.* **129,** 114707 (2008).
39. Anikeenko, A. V. & Medvedev, N. N. Polytetrahedral nature of the dense disordered packings of hard spheres. *Phys. Rev. Lett.* **98,** 235504 (2007).
40. Meijer, E. J. & Frenkel, D. Melting line of Yukawa system by computer simulation. *J. Chem. Phys.* **94,** 2269–2271 (1991).
41. Zahn, K. & Maret, G. Dynamic criteria for melting in two dimensions. *Phys. Rev. Lett.* **85,** 3656–3659 (2000).

Author contributions

P.T. and L.X. conceived and designed the experiments, P.T. performed the experiments, P.T., N.X. and L.X. analysed the data, P.T. developed the new approach of local bond order analysis, and P.T. and L.X. wrote the paper.

Additional information

Supplementary information is available in the online version of the paper. Reprints and permissions information is available online at www.nature.com/reprints. Correspondence and requests for materials should be addressed to L.X.

Competing financial interests

The authors declare no competing financial interests.